Heteroepitaxial growth of sp 2 -hybridized boron nitride multilayer on nickel substrates by CVD: the key role of the substrate orientation

Henri Prevost, Amandine Andrieux-Ledier, Nelly Dorval, Frédéric Fossard, Jean Sébastien Mérot, Léonard Schué, Alexandre Plaud, Eva Héripré, Julien Barjon, Annick Loiseau

▶ **To cite this version:**

Henri Prevost, Amandine Andrieux-Ledier, Nelly Dorval, Frédéric Fossard, Jean Sébastien Mérot, et al.. Heteroepitaxial growth of sp 2 -hybridized boron nitride multilayer on nickel substrates by CVD: the key role of the substrate orientation. 2D Materials, 2020, 7 (4, 045018), pp.1-10. 10.1088/2053-1583/aba8ad . hal-02969129

HAL Id: hal-02969129
https://hal.science/hal-02969129

Submitted on 16 Oct 2020

HAL is a multi-disciplinary open access archive for the deposit and dissemination of scientific research documents, whether they are published or not. The documents may come from teaching and research institutions in France or abroad, or from public or private research centers.

L'archive ouverte pluridisciplinaire **HAL**, est destinée au dépôt et à la diffusion de documents scientifiques de niveau recherche, publiés ou non, émanant des établissements d'enseignement et de recherche français ou étrangers, des laboratoires publics ou privés.

Heteroepitaxial growth of sp^2-hybridized boron nitride multilayer on nickel substrates by CVD: the key role of the substrate orientation

H. Prevost[1], A. Andrieux-Ledier[2], N. Dorval[2], F. Fossard[1], J.S. Mérot[1], L. Schué[1, 3], A. Plaud[1, 3], E. Héripré[4], J.Barjon[3] and A.Loiseau[1]

[1] LEM, UMR 104 CNRS-ONERA, Université Paris Saclay, F-92322 Châtillon - France

[2] DPHY, ONERA, Université Paris Saclay, F-92322 Châtillon - France

[3] GEMaC, CNRS, UVSQ, Université Paris-Saclay, Versailles - France

[4] MSSMat, CNRS - CentraleSupélec, Université Paris-Saclay, 91190 Gif-sur-Yvette - France

Abstract

sp^2-hybridized boron nitride is identified as a strategic material for many purposes related to the integration of graphene and 2D materials in devices and the fabrication of van der Waals heterostructures. Thus, it becomes mandatory to have scalable synthesis and characterization procedures for providing suitable and reliable boron nitride material according to these identified needs. We report here on the growth of sp^2-hybridized boron nitride film on polycrystalline nickel substrate by chemical vapor deposition with borazine as precursor. We propose a complete study of the influence of the underlying nickel grain orientation on the BN structure layers, in terms of thickness, crystallographic orientation, domain size and stacking. We show the heteroepitaxial growth of continuous, single crystalline hexagonal boron nitride multilayer film on nickel (111) -like grains. We highlight its ABC stacking sequence with AB stacking faults and show how it impacts the Raman and cathodoluminescence spectra.

1. Introduction

After the discovery of graphene in 2004, and its consequences in the field of nanoscience and nanomaterials, there has been a growing interest in the integration of 2D materials in devices based on van der Waals (vdW) heterostructures [1,2]. sp^2-hybridized boron nitride (sp^2-BN) has been identified as one of these strategic materials. It is the graphene counterpart, with its B and N atoms arranged in honeycomb lattice which can crystallize into two different polymorphs [3]: hexagonal phase (AA' stacking sequence - space group: $P6_3/mmc$) or rhombohedral phase (ABC stacking sequence - space group: R3m). Due to its specific properties - large bandgap (> 6 eV), atomic flatness, free from dangling bonds, chemical inertness, low dielectric screening and small lattice mismatch with graphene (1,8%) [1], sp^2-BN has emerged in the recent years as an ideal material as it can fulfill different functions in vdW heterostructures-based devices: capping layers to provide clean encapsulation environment [4] and enhancing physical properties such as luminescence properties of Transition Metal DiChalcogenides (TMDC) [5], supporting insulating materials to preserve electronic properties of graphene [6,7] or dielectric inter-layer in vertical electronic devices [8]. The performances and the properties of these devices can be directly impacted by the structural characteristics and the quality (roughness, thickness, size domain, stacking sequence, level and nature of the impurities, stacking fault density or crystallinity at the macro- and nanoscale) of the BN film [9]. Therefore it is highly desirable to be able to precisely control and identify all these features via the synthesis conditions and appropriate characterization techniques, respectively. Throughout the literature, the added value of using BN layers and films on the performances of graphene and other 2D materials is demonstrated with exfoliated flakes from bulk BN crystals. These AA'-stacked BN sources, obtained by high pressure-high temperature (HPHT) process [10,11] or by polymer-derived-ceramic (PDC) routes [12] offer the decisive advantage to be single crystalline, atomically flat and to contain a very low level of defects and impurities [9]. However, using these bulk sources implies to operate a mechanical or liquid phase exfoliation process [13,14] which is source of several limitations, the main of which being the limited lateral size of extracted exfoliated flakes partly due to the process itself and partly due to the small size of the available bulk crystals, the lack of

control of the number of layers and the structural and chemical degradation which may be induced by the process.

Therefore, it is mandatory but still a great challenge to have suitable and reliable synthesis procedure able to produce wafer-scale sp^2-BN layers and substrates. Indeed sp^2-BN is not a natural material in contrast to its graphite counterpart and the HPHT process is, to date, the most reliable route to millimeter size single crystals. Chemical Vapor Deposition (CVD) on a metallic substrate is a very promising and versatile synthesis route. Several methods including CVD under ultra-high vacuum on single crystalline transition metal [15] and also CVD on polycrystalline foils have been reported to achieve large scale BN monolayers up to 0.5 mm [16–20]. However the growth of flat BN multilayer with thickness ranging from a few to a few tens of nanometers is highly demanded to be used as substrate or capping layers. Many combinations of polycrystalline substrates (Cu, Ni, Pt…), precursors (borazine, ammonia borane…), pressure and temperature have been explored and different strategies have been worked out to control the structure and the quality of the BN film and to understand the growth mechanism. Polycrystalline copper substrates in general lead to multilayered BN films with variable roughness and a turbostratic character of the stacking whatever the thickness [21–23]. Even the quality and the structure of the BN film grown on polycrystalline copper is quite different from that of the exfoliated bulk BN single crystal, early work on "all-CVD" devices with this type of materials show promising results [24–26].

More promising is the use of iron and nickel substrates for the growth. Large areas of higher quality multilayer BN films can be grown on polycrystalline Fe substrates, provided to operate a slow cooling rate, following the exposure to boron and nitrogen precursors in a high temperature stage [27]. This process is made possible by the ability of Fe to solubilize B and N at high temperature. As a result, the growth proceeds by diffusion of B and N in Fe film at high temperature; then they segregate at the surface during the cooling to let BN domains nucleate and grow. This precipitation-driven growth during cooling can be controlled and limited to a monolayer by the saturation of the Fe substrate with nitrogen via NH_3 exposure prior to the growth step [28].

Particular attention has been paid to the synthesis on nickel substrates, due to their ability to catalyze the synthesis of well crystallized mono-, few- and multilayer BN [21,29]. According to the solubility of B and N in Ni, growth of BN layers is proposed to follow a similar precipitation-driven process during cooling as on Fe [30]. Further, the film thickness can be limited to one or two layers with a lateral domain size up to 100µm via the formation of an intermediate boron oxide phase then reduced by carbon on the interior surface of a nickel enclosure, inhibiting the diffusion of B and N atoms into the bulk [31]. Interestingly, several groups have investigated the influence of the underlying nickel grain orientation on the BN growth in terms of kinetics, coverage and thickness, but with contradictory results. Lee et al. highlight different growth kinetics with respect to the nickel crystalline orientations leading to different thicknesses and morphologies of the BN film, i.e. no growth on Ni (111), low growth rate / thin-discontinuous film on Ni (101) and faster growth / flat- thick layered structure on Ni (100) [32]. Cho et al. [33] observe an increase of the growth rate on (111), (100) and (101) orientations in that order, attributed to the differences of their surface energy and sticking coefficient of the boron, nitrogen and hydrogen atoms. In a more recent study, (110) nickel faces were also observed to provide the highest growth rate, but followed by (111) and (100) faces [34]. The authors attribute these differences to the dependence of the surface and bulk diffusion of B and N atoms on the nickel orientation which affects the diffusion/precipitation and the layer-by-layer growth.

Here, we focus on the growth of multi-layered films on polycrystalline Ni foils and thoroughly investigate the influence of the nickel grain crystalline orientation on the BN film structure and quality, in terms of thickness, crystallographic orientation, domain size and stacking sequence. To that aim, we have combined a panel of characterization techniques: Scanning Electron Microscopy- Electron Backscatter Diffraction (SEM-EBSD) mapping, Raman spectroscopy measurements, High-Resolution Transmission Electron Microscopy (HRTEM) imaging, Scanning TEM - High Angle Annular Dark Field (STEM-HAADF) imaging, electron diffraction and cathodoluminescence. In such a way, we show that, under our growth conditions, different growth modes occur leading to nanocrystalline BN films on Ni (001)-like grains but heteroepitaxial growth on Ni (111)-like grains, with a domain size as large as the underlying nickel grain.

We highlight the ABC stacking sequence of the multilayer BN film with AB stacking fault and we show how it impacts the Raman and cathodoluminescence spectra.

2. Methods

2.1. CVD growth of boron nitride on polycrystalline nickel

The CVD growth of multilayer BN film was carried out in a homemade hot-wall reactor, consisting of a 7-inch chamber with induction heating. The gases flow through the reactor from the bottom alongside the metallic substrate. Hydrogen (Air Liquide, 99.9999%) is used as a carrier gas for the BN precursor, borazine ($B_3N_3H_6$, Katchem, > 98%). The flow rate is easily controlled by a system of mass flow controllers. To lower the vapor pressure and thus avoid gas flash in the CVD chamber, borazine is maintained at 0°C with a chiller. A cold trap was installed to prevent the damage of the scroll pump with borazine.

Polycrystalline nickel foils (Goodfellow, 25 µm thick, 99.999%) are used as a substrate for the CVD growth. In a typical process, the substrate is placed in the CVD reactor pumped-down to low pressure (10^{-3} mbar). Then the furnace is ramped up to 600°C under vacuum, without gas flow. A pre-annealing step of the Ni foil takes place under these conditions for 90 minutes. Then the chamber is cooled down to room temperature. The pumping and heating steps are reiterated, up to 600°C without gas, then up to 1000°C under 50 sccm of hydrogen, temperature at which the nickel foil is annealed for 30 minutes, under 50 sccm of hydrogen and a regulated pressure of 0.3 mbar. Then, 2.5 sccm of borazine is introduced in the reaction chamber at 1000°C, under 50 sccm of hydrogen, at a regulated pressure of 0.3 mbar during 20 minutes. Finally, the chamber is cooled down to room temperature, at a rate of 13°C/minutes, under hydrogen atmosphere until 450°C.

2.2. TEM sample preparation

The BN films were first characterized in their native state and then transferred onto TEM grid (SPI - Au Quantifoil - 1.2 µm holey amorphous carbon film) via a polymer-free transfer technique [35]. The multilayer nature of the as-grown BN allows us to transfer without any holder. The nickel foil was etched with a commercial solution (TFB Nickel Etchant, Transene) for several hours. The BN film floating at the surface was rinsed with deionized water and fished with the TEM grid. Finally the BN/TEM grid substrate was slowly heated up to 120°C to remove excess of water.

60 nm-thick TEM lamellas were prepared on a FEI Helios 660 dual-beam microscope combining a field emission gun (FEG) scanning electron microscope (SEM) with an advanced focused ion beam (FIB) column operating at 30 kV. We followed a two platinum deposition steps to avoid amorphization of the BN film. A first deposit is obtained using the electron beam to crack the Pt precursor and the second one using the ion beam to achieve the desired Pt thickness [36].

2.3. Characterization

SEM imaging and EBSD mapping were performed on the FEI Helios 660 dual-beam microscope equipped with a EDAX Hikari XP EBSD camera at 2 kV and 20 kV respectively. EBSD acquisition has been performed with EDAX-TEAM software.

Micro-Raman measurements were performed at room temperature with a Renishaw Invia spectrometer with a 473 nm Co laser source, with a 100X objective, a 1200 lines/mm grating, a power level below 1 mW.

Samples transferred on holey carbon TEM grids or prepared by FIB thinning were examined in a Zeiss Libra 200 MC equipped with an electrostatic CEOS monochromator, an in-column Ω filter and a Gatan ultrascan 1000 CCD camera. The microscope was operated at 40kV for EELS to reduce beam damage on thin films and increase the performances of the monochromator. As a result, the energy resolution, measured

at the full width at half maximum of the elastic peak, is below 150 meV. The measurement of the film thickness is extracted from the contrast profile of images recorded in the STEM-HAADF mode at 80 keV, using a contrast calibration performed with BN samples with known thicknesses so as to get the thickness directly from the intensity of the scattered signal. The stacking sequence on FIB lamellae has been determined using the High Resolution phase contrast imaging mode (HRTEM) at 200 keV providing a resolution limit below 150 pm.

Gatan Digital Micrograph 2 software was used for acquisition and analysis of HRTEM images treatment. Electron diffraction simulations were obtained using SingleCrystal software and schematic illustrations of the stacking sequence were obtained using Crystal Maker software.

Cathodoluminescence (CL) spectra were acquired with a JEOL7001F field emission gun scanning electron microscope coupled to an achromatic Horiba Jobin-Yvon spectrometer as described by Schué et al. [37] The sample was mounted on a Gatan cooling stage allowing for a CL analysis at liquid helium temperature, the sample holder being at 5K. CL spectra were recorded from BN films transferred on a TEM grid, in scanning mode at 80k magnification using a (5 kV, 1 nA) incident electron beam.

3. Results and discussion

3.1. Boron nitride morphologies versus nickel grain orientation

As mentioned in the experimental section, the synthesis of multilayer BN film follows a typical CVD sequence, including heating/annealing/growth and cooling down steps. The pre-annealing step at 600°C aims at removing some of the carbon species on the nickel substrate [38] ([C] > 30 ppm in 99.999% Ni) that could create a contamination of the BN film during its synthesis. The annealing stage at 1000°C under hydrogen atmosphere promotes the enlargement of the nickel grain size and the reconstruction of the surface morphology [39] while removing the native oxide layer [40]. Then the substrate is exposed to the borazine, which presents an ideal isostœchiometry and thus does

not introduce any by-product during its decomposition unlike ammonia-borane [16,41]. The furnace is then cooled down slowly to room temperature.

SEM images of the sample are taken to get a first insight of the BN growth morphology. Figure 1a shows the nickel substrate after BN growth revealing two different surface aspects, one striated and another much rougher. This observation suggests a significant role of the underlying nickel grain orientation on the BN growth mode, as already observed by Lee et al.[42]. EBSD was performed to clarify this point. Figure 1b shows the EBSD mapping corresponding to the SEM image, with the crystalline orientation color scale in inset. As the BN film is very thin (< 20 nm), its signal cannot be detected by standard EBSD technique. The observed signal is that of the nickel substrate. A random and high roughness is observed on surfaces close to the (100) orientation (in red). On the contrary (111)-like grains (in blue) present a flatter morphology marked by parallel striations. They are related to the formation of step bunches at the nickel surface (Figure SI1) during the heating of the substrate prior to the growth [39].

To achieve further information on the correlation between the structure of the film and the underlying Ni grain, the film was transferred from the nickel foil onto a TEM grid via the direct technique described in the experimental section. A low magnification TEM image (Figure SI2) shows an example of a large area transfer, over the whole TEM grid. TEM image at higher magnification (Figure 1c) reveals a continuous film consisting in a pattern of areas, with different contrasts. This is characteristic of variations in the BN film thickness, which is a footprint imprint of the Ni grain microstructure on which the film has grown. Consistently with SEM analyses, we clearly identify two kinds of morphologies depicted in Figure 1d, one assigned as ‘flat’, characterized by parallel striations consecutive to a growth on Ni (111) surfaces and the second one assigned as ‘rough’ resulting from a growth on Ni (001) surfaces. These two kinds of morphologies are analyzed in details in the next sections.

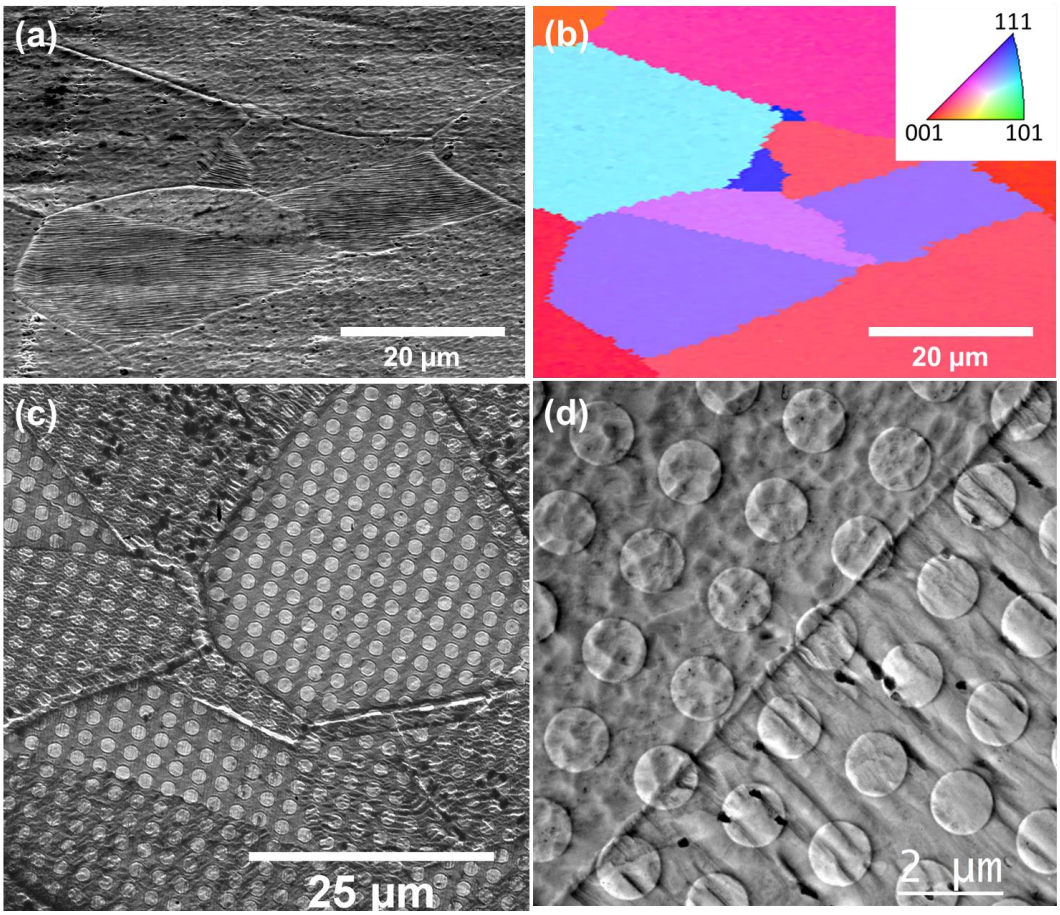

Figure 1 : SEM image (a) with (b) EBSD related orientation map (with a 70° tilt angle) of the nickel foil after the exposition to borazine at 1000°C. In inset, the color scale for the crystalline orientation of the sample surface: low index surfaces are plotted in red for (100), blue for (111) and green for (101), while intermediate colors correspond to vicinal surfaces. (c) TEM image showing the print of the nickel grain boundaries in the BN film. (d) Higher magnification TEM image showing rough (left) and flat (right) BN morphologies. Hole pattern comes from the underlying carbon skin of the TEM grid.

3.3. Multilayer boron nitride on nickel (001)-like grains

STEM-HAADF imaging and electron diffraction are performed on BN transferred on the TEM grid. Low magnification STEM-HAADF images (Figure 2a), sensitive to the thickness, reveal that the film grown on Ni(001)–like grains consist of an agglomerate of islands with an appearance of

cotton flowers. Average lateral size of the islands is around 0.6 µm. The thickness variation within the islands - depicted by a square in Figure 2a - is measured by the STEM-HAADF technique (see details in Characterization part) and is presented in Figure 2b. This thickness mapping highlights significant variations from 0 to 10 nm within an island and a discontinuity between the islands. This discontinuity is clearly shown in the magnified image of Figure 2c of a junction between three islands. Selected Area Electron Diffraction (SAED) patterns were recorded in three neighboring islands circled in Figure 2c. Each island produces a six-fold symmetry pattern corresponding to a single BN domain in basal orientation (Figure 2d, e and f). The rotation between patterns indicates a lack of orientational coherence between the islands. We conclude that boron nitride films grown on (100) -like grains are polycrystalline with sub-micrometer grain sizes, randomly oriented and disconnected each other. They are clearly not appropriate for a use as either a substrate either a capping protective medium as sought.

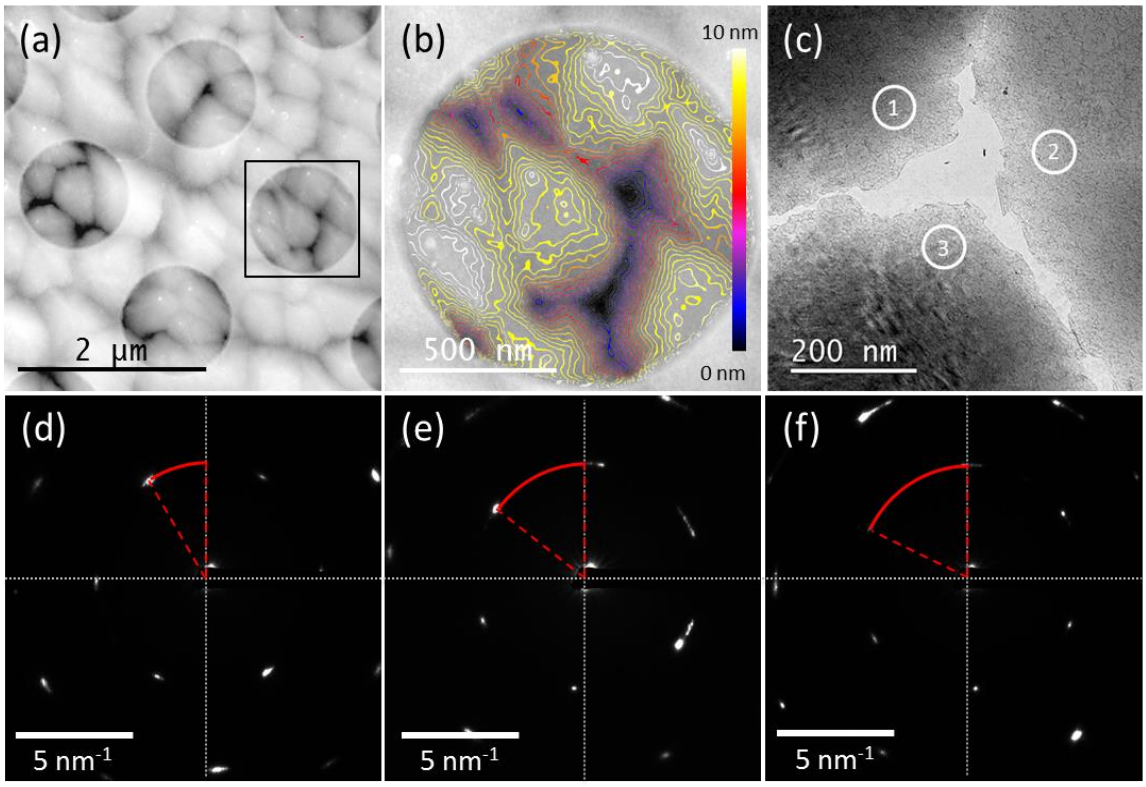

Figure 2 : Polycrystalline BN film grown on Ni (001) by CVD ; (a) Low-magnification STEM-HAADF image (b) STEM-HAADF image of the area delimited by the black line square, superimposed with a mapping drown in contour lines of the thickness. (c) TEM image at a three islands junction. The circled numbers 1, 2 and 3 indicate the location where the SAED patterns (d), (e) and (f) were

recorded, respectively. The random orientation of islands (rotations in red in the SAED patterns) evidences the polycrystalline character of the BN film.

3.4. Multilayer boron nitride on nickel (111) -like grains

3.4.1. BN film / Ni (111) interface and stacking sequence determination

In order to achieve information on the BN film on the Ni (111)-like grains, we prepared a TEM cross-section by FIB of a (111) nickel grain previously identified by SEM-EBSD. Figure 3a presents a high magnification HRTEM image of the cross-section. As specified in the experimental section, the top platinum layers have been deposited in order to protect the BN film and preserve its integrity during the milling process by FIB. We first checked the underlying Ni grain surface is (111) as expected from EBSD analysis. Second the BN film is conform to the underneath nickel like grain, with a flat and sharp interface. The BN film is continuous and consists of a regular stack of layers through the entire thickness, with an interlayer distance of 0.33nm, as expected for sp^2-hybridized BN.

The edge-on view also provides a direct visualization of the stacking sequence in sp^2-hybridized BN film. The high magnification TEM images are filtered and compared to simulated TEM images and atomic potential superimposed with Crystal Maker simulation for a better clarity. The positions of white dots are related to the position of a boron-nitrogen pair of atomic columns that cannot be distinguished each other with respect to our resolution. Despite this lack of resolution, a proper identification of the stacking arrangement of the BN layers can be addressed. We could identify two different configurations. Depending on the regions, each layer n is equivalent either to the n+3 layer (Figure 3b) or to the n+2 layer (Figure 3c). These periodicities are characteristic of the ABC and AB stacking sequences respectively. A statistical analysis made over all HRTEM images indicates that the BN stacking sequence is more likely to be of AB type rather than ABC type. .

As mentioned in the introduction, according to the BN phase diagram [43], the rhombohedral phase, corresponding to the ABC stacking sequence, is one of the two stable sp^2 BN phases at atmospheric pressure. Experimentally, both ABC and AA' (hBN) stacking sequence have been obtained under standard or low pressure growth conditions [44,45]. According to Sato et al. "the factor determining the relative amounts […] of these phases in synthetic products will not be the PT [i.e. pressure and temperature] condition but the growth mechanism" [46] and recent calculations of Pedersen et al. suggest that the change in BN polytype depends on lattice-mismatch-induced stress relaxation [47]. In our case, the epitaxial relationship of BN on Ni(111) tends to favor the ABC stacking by a mechanism which remains to be elucidated.

AB stacking sequence is not a phase but rather a stacking fault of the rhombohedral phase. The presence of these stacking faults in large amount in our BN film can be related to the irregular nickel surface. Indeed, the aforementioned (111) grains are stepped (111) surfaces at the nickel grain microscale (See SEM image Figure 1 and Figure SI1). The nickel terraces can thus induce stress in the BN film and be at the origin of the observed AB stacking faults in ABC-stacked boron nitride film.

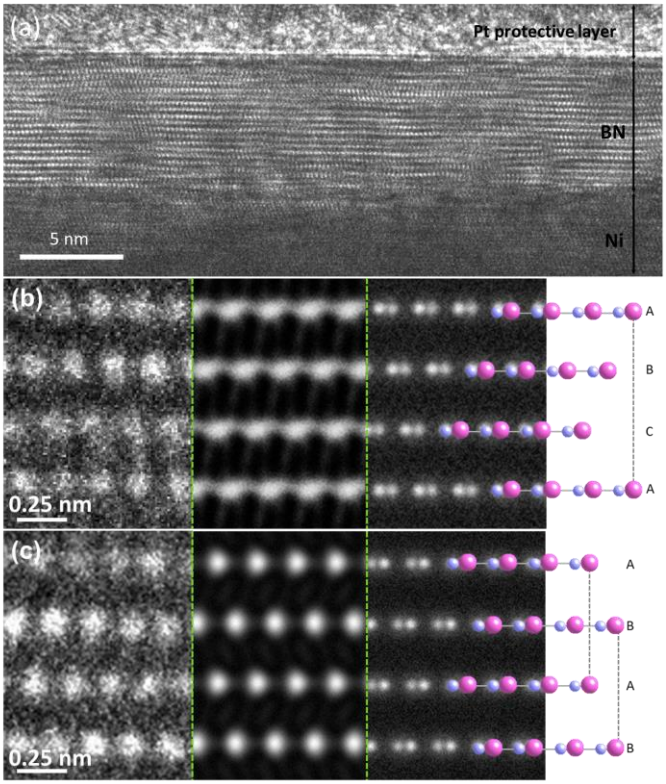

Figure 3: (a) HRTEM image of the hBN lamellae in edge view configuration evidencing the multilayer stacking *and the regularity of the sp^2-BN film along the entire thickness and surface. High magnification filtered TEM images, simulated TEM images and atomic potential superimposed with Crystal Maker simulation of (b) ABC and (c) AB stacking sequence*

3.4.2. Orientation relationship between the BN film and the nickel (111) substrate

In order to evaluate whether an orientation relationship exists between the boron nitride film and nickel (111) grain, we have examined selected area electron diffraction (SAED) and fast Fourier transform (FFT) from HRTEM images recorded in in-plane and cross-section TEM samples. The lattice parameters of BN with an AB stacking sequence are used for the indexation: a= 2.5 Å, c= 6.66 Å (space group: P-6m2). The lattice parameter of nickel used for the indexation is a=3.5 Å (space group: Fm-3m).

Figure 4a presents a plane-view TEM image showing a flat and continuous BN film identified as grown on Ni (111). Selected-area electron diffraction (SAED) patterns (Figure 4b, c and d), recorded at three different locations (Figure 4a) show the six-fold symmetry pattern characteristic of sp^2-boron nitride in basal orientation and indexed in the hexagonal unit cell, indicating that the BN atomic planes are stacked parallel to the Ni (111) surface. In contrast to BN areas grown on nickel (001) orientation, no rotation between the three diffraction patterns is observed, attesting the presence of a single orientation of the BN domain over the entire nickel (111) -like grain. This suggests an epitaxial relationship between the boron nitride layer and the Ni (111) surface. Such behavior is likely to occur indeed given the small lattice mismatch of 0.5% between sp^2-BN (00.1) and nickel (111) (lattice constants of 2.50 Å and 2.49 Å, respectively) [48]. The presence of (10-10) diffraction spots located at 4.65 nm^{-1}, corresponding to a 2.16 Å inter-reticular distance, confirms the presence of AB stacking faults since ABC stacking sequence (rBN) generates diffraction extinction for these distances [9].

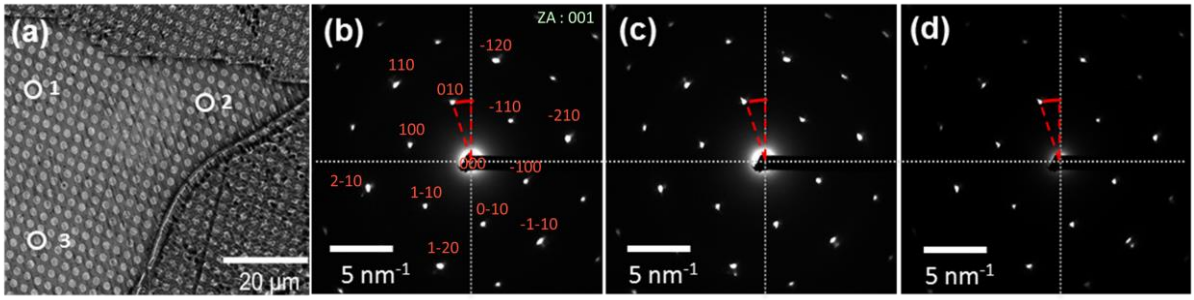

Figure 4 : (a) in-plane TEM image of a flat BN grain. White circles indicate the location in the boron nitride grain grown on (111) Ni surface where SAED patterns were recorded, (b), (c) and (d) respectively. The lack of rotation evidences the monocrystalline character of the BN layer.

In order to determine the complete orientation relationship between the substrate and the BN film, we examined FFT patterns of HRTEM images (Figure 5a) recorded on Ni grain (Figure 5b) and on BN layers (Figure 5c) in the cross-sections cut by FIB. Indexation of the patterns and of the corresponding zone axes is supported by electron diffraction simulation (Figure 5d and f) using SingleCrystal software. According to these simulations, we identify that the $[0\bar{1}10]$ zone axis of the BN film is parallel to the $[1\bar{1}0]$ zone axis of the nickel substrate and that [111] direction of nickel is parallel to the [0001] direction of the hexagonal BN layers. We can therefore conclude that the epitaxy relationship between BN and nickel can be defined as:

$$[111]_{Ni} \,||\, [0001]_{BN}$$

$$[1\bar{1}0]_{Ni} \,||\, [0\bar{1}10]_{BN}$$

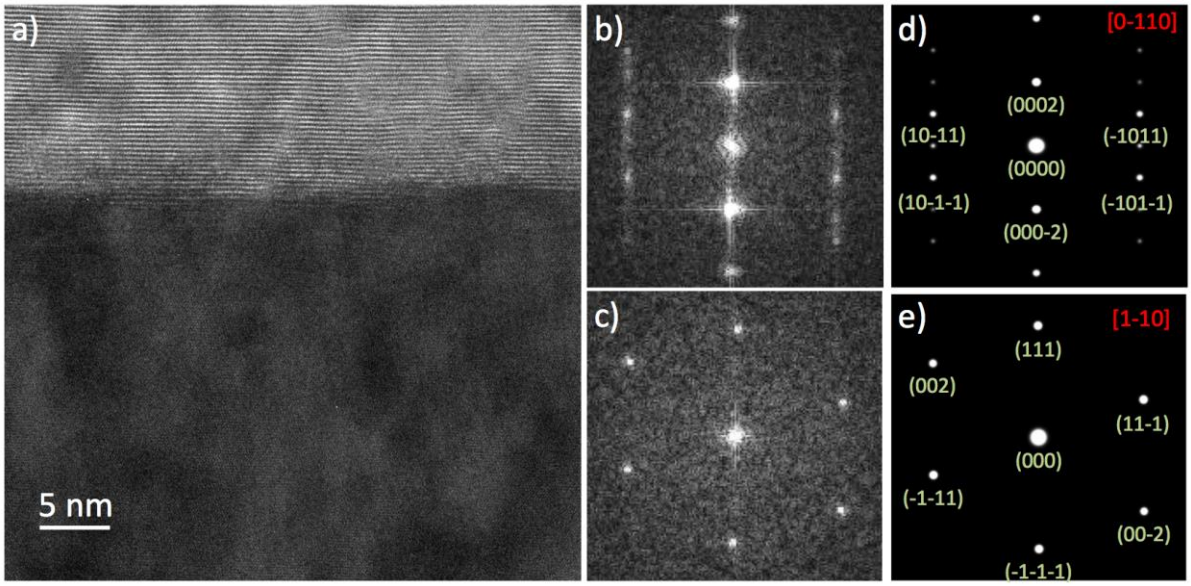

Figure 5 : HRTEM analysis of the BN/ Ni(111) interface: (a) HRTEM image, (b) and (c) are FFT of the BN and nickel part, respectively. Electron diffraction simulation of AB-stacked BN (d) and Ni (e) in [0-110] and [1-10] zone axis respectively.

3.4.3. Raman and cathodoluminescence spectra of multilayer BN film on Ni(111)

Raman spectroscopy has been used to probe the BN film at a macroscopic scale. We performed a series of ten measurements directly on the as grown BN film on nickel (111) -like grain. The typical Raman spectrum (Figure 6a) exhibits two peaks. The most intense one is detected between 1370.0 and 1371.5 cm^{-1} with a full width half maximum (FWHM) ranging from 37 to 42 cm^{-1}. This peak is well documented in the literature and corresponds to the in-plane vibration mode (E_{2g}) in sp^2-hybridized BN whatever the stacking sequence [49–51]. These FWHM values are coherent with the values given in the literature for bulk or CVD rBN, i.e. 30 cm^{-1} [52,53] and 40 cm^{-1} [50] . The exact origin of the broadening of the E_{2g} peak is, up to now, unknown. As for hBN, it can be correlated to defects (such as the large quantity of AB stacking faults) or strain in the BN film [54,55].

The lower frequency peak, 804-810 cm^{-1}, corresponds to the out-of-plane, interlayer breathing mode (A_1), not visible for the AA' and AB stacking sequence [49,56] but Raman active for the ABC stacking sequence [46,50,51]. Special consideration should be taken in the attribution of this peak

whose position also corresponds to B_2O_3 signal [57]. In our case, the EELS characterization (presented in the Figure SI3) has excluded the presence of any oxide in the as-grown BN layers. The signal is then attributed to the fraction of rhombohedral structure previously identified by HRTEM imaging. The FWHM of the peak range between 25 and 45 cm^{-1} consistently with the only experimental value available in the literature at 790 cm^{-1} with a FWHM of 35 cm^{-1} for rBN crystallites [50].

The BN films grown on nickel (111)-like grain were also investigated by cathodoluminescence at low temperature (5K) after being transferred on a holey carbon TEM grid. The CL spectrum, shown on Figure 6b, is dominated by a peak close to 230 nm (5.4 eV) in the near band edge region, relatively broad (FWHM = 170 meV) compared to the AA'-hBN intrinsic luminescence lines (FWHM=5 meV) in reference hBN single crystals [9]. Emissions in this range have been reported for turbostratic BN [58] or multi-walled BN nanotubes [59,60], but also for rBN nanoplates [61] attributed, so far to excitons bounded on structural defects or impurities. It is probably also the case here, but the detailed TEM analysis further points the 230 nm luminescence signal as related to the AB stacking in boron nitride.

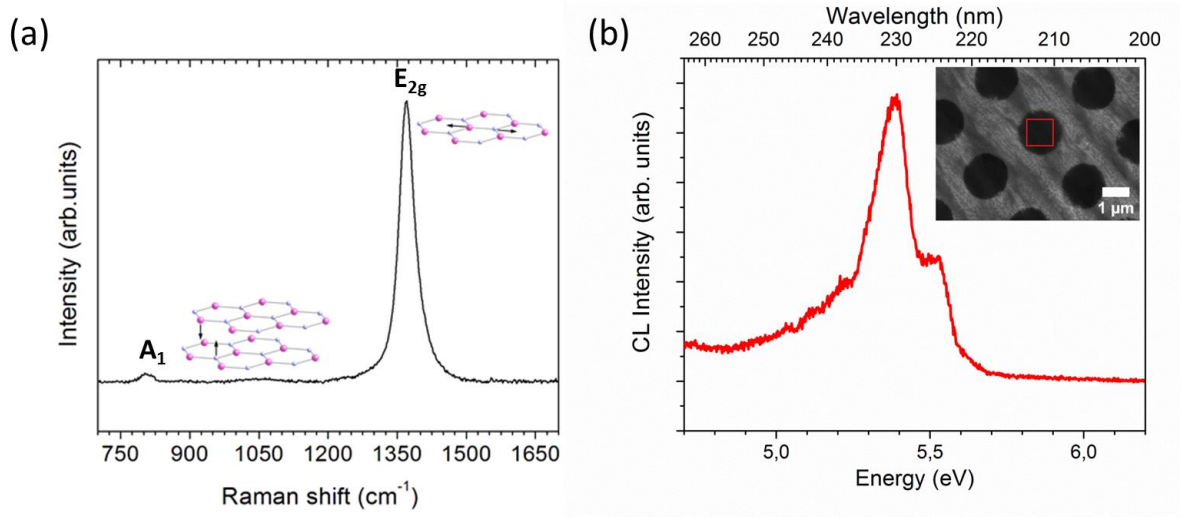

Figure 6: (a) Typical Raman spectrum recorded on BN film grown on Ni (111) showing both the in–plane vibration mode (E_{2g}) at 1370 cm^{-1} and the layer breathing mode (A_1) at 808 cm^{-1}. (e) Cathodoluminescence spectrum at T=5 K recorded on the suspended BN/Ni (111) epilayer, as shown with the SEM image in inset.

4. Conclusion

To summarize, we present a complete study of the influence of the nickel orientation on the BN quality and structural characteristic grown by chemical vapor deposition. Under our conditions, the growth on nickel (001)-like surface leads to polycrystalline BN film with sub-micrometer grain sizes, randomly oriented. The multilayer sp^2-hybridized BN film obtained on the nickel (111)-like surface are single crystalline and continuous. The BN film is conformal to the underneath nickel grain, with a flat and sharp interface and we highlight its heteroepitaxial growth by a mechanism which remains to understand. We show that the regular stack of layers follows an ABC stacking sequence, characteristic of the rhombohedral phase, with AB stacking faults. Finally, we identify the rBN phase on the Raman spectra, with the peak characteristic of the interlayer-breathing-mode (A_1 mode around 800 cm^{-1}), theoretically predicted to be Raman active for other stacking sequences than AA'. This detailed analysis provides insights and guidelines for further optimization of the synthesis conditions to planar and single crystalline multilayer BN film on nickel (111) monocrystalline substrate, with the quality required for the integration in devices as top or bottom layer.

Acknowledgement

J.C. Daux, J.F. Justin and B. Passilly (Département Matériaux et Structure - ONERA) are warmly acknowledged for their precious technical support on CVD set-up. Authors thank H.Amara, F. Ducastelle and L.Sponza (LEM – CNRS/ONERA) for very helpful discussions.

This work was carried out within the MATMECA consortium and supported by the ANR under contract number ANR-10-EQPX-37. It has benefited from the facilities of the Laboratory MSSMat (UMR CNRS 8579), CentraleSupélec, France. The research leading to these results has received funding European Union's Horizon 2020 research and innovation program under grant agreements No. 696656 (Graphene Core 1) and No 785219 (Graphene Core 2) and from the ANR french program under the grant agreement No. ANR-14-CE08-0018 (project GoBN) and from ONERA

References

[1] T. Niu, A. Li, From two-dimensional materials to heterostructures, Prog. Surf. Sci., 90 (2015) 21–45.

[2] A.K. Geim, I.V. Grigorieva, Van der Waals heterostructures, Nature, 499 (2013) 419–425.

[3] K. Luo, X. Yuan, Z. Zhao, D. Yu, B. Xu, Z. Liu, Y. Tian, G. Gao, J. He, New hexagonal boron nitride polytypes with triple-layer periodicity, J. Appl. Phys., 121 (2017).

[4] G.C. Constantinescu, N.D.M. Hine, Multipurpose Black-Phosphorus/hBN Heterostructures, Nano Lett., 16 (2016) 2586–2594.

[5] F. Cadiz, E. Courtade, C. Robert, G. Wang, Y. Shen, H. Cai, T. Taniguchi, K. Watanabe, H. Carrere, D. Lagarde, M. Manca, T. Amand, P. Renucci, S. Tongay, X. Marie, B. Urbaszek, Excitonic linewidth approaching the homogeneous limit in MoS2-based van der Waals heterostructures, Phys. Rev. X, (2017).

[6] L. Banszerus, M. Schmitz, S. Engels, J. Dauber, M. Oellers, F. Haupt, K. Watanabe, T. Taniguchi, B. Beschoten, C. Stampfer, Ultrahigh-mobility graphene devices from chemical vapor deposition on reusable copper, Sci. Adv., 1 (2015).

[7] C.R. Dean, A.F. Young, I. Meric, C. Lee, L. Wang, S. Sorgenfrei, K. Watanabe, T. Taniguchi, P. Kim, K.L. Shepard, J. Hone, Boron nitride substrates for high-quality graphene electronics, Nat. Nanotechnol., 5 (2010) 722–726.

[8] M. Parzefall, P. Bharadwaj, A. Jain, T. Taniguchi, K. Watanabe, L. Novotny, Antenna-coupled photon emission from hexagonal boron nitride tunnel junctions, Nat. Nanotechnol., 10 (2015) 1058–1063.

[9] L. Schué, I. Stenger, F. Fossard, A. Loiseau, J. Barjon, Characterization methods dedicated to nanometer-thick hBN layers, 2D Mater., 4 (2017).

[10] T. Taniguchi, K. Watanabe, Synthesis of high-purity boron nitride single crystals under high pressure by using Ba-BN solvent, J. Cryst. Growth, (2007).

[11] K. Watanabe, T. Taniguchi, H. Kanda, Direct-bandgap properties and evidence for ultraviolet

lasing of hexagonal boron nitride single crystal, Nat. Mater., (2004).

[12] Y. Li, V. Garnier, C. Journet, J. Barjon, A. Loiseau, I. Stenger, A. Plaud, B. Toury, P. Steyer, Advanced synthesis of highly crystallized hexagonal boron nitride by coupling polymer-derived ceramics and spark plasma sintering processes - Influence of the crystallization promoter and sintering temperature, Nanotechnology, (2019).

[13] J.N. Coleman, M. Lotya, A. O'Neill, S.D. Bergin, P.J. King, U. Khan, K. Young, A. Gaucher, S. De, R.J. Smith, I. V. Shvets, S.K. Arora, G. Stanton, H.Y. Kim, K. Lee, G.T. Kim, G.S. Duesberg, T. Hallam, J.J. Boland, J.J. Wang, et al., Two-dimensional nanosheets produced by liquid exfoliation of layered materials, Science (80-.)., (2011).

[14] D. Pacile, J.C. Meyer, Ç. Girit, A. Zettl, The two-dimensional phase of boron nitride: Few-atomic-layer sheets and suspended membranes, Appl. Phys. Lett., 92 (2008).

[15] W. Auwärter, Hexagonal boron nitride monolayers on metal supports: Versatile templates for atoms, molecules and nanostructures, Surf. Sci. Rep., (2019).

[16] J.H. Park, J.C. Park, S.J. Yun, H. Kim, D.H. Luong, S.M. Kim, S.H. Choi, W. Yang, J. Kong, K.K. Kim, Y.H. Lee, Large-area monolayer hexagonal boron nitride on Pt foil, ACS Nano, 8 (2014) 8520–8528.

[17] R. Wang, D.G. Purdie, Y. Fan, F.C.P. Massabuau, P. Braeuninger-Weimer, O.J. Burton, R. Blume, R. Schloegl, A. Lombardo, R.S. Weatherup, S. Hofmann, A peeling approach for integrated manufacturing of large monolayer h-BN crystals, ACS Nano, 13 (2019) 2114–2126.

[18] R.Y. Tay, M.H. Griep, G. Mallick, S.H. Tsang, R.S. Singh, T. Tumlin, E.H.T. Teo, S.P. Karna, Growth of large single-crystalline two-dimensional boron nitride hexagons on electropolished copper, Nano Lett., 14 (2014) 839–846.

[19] Q. Wu, J.-H. Park, S. Park, S.J. Jung, H. Suh, N. Park, W. Wongwiriyapan, S. Lee, Y.H. Lee, Y.J. Song, Single Crystalline Film of Hexagonal Boron Nitride Atomic Monolayer by Controlling Nucleation Seeds and Domains, Sci. Rep., 5 (2015) 16159.

[20] L. Wang, B. Wu, L. Jiang, J. Chen, Y. Li, W. Guo, P. Hu, Y. Liu, Growth and Etching of Monolayer Hexagonal Boron Nitride, Adv. Mater., (2015).

[21] A. Ismach, H. Chou, D.A. Ferrer, Y. Wu, S. McDonnell, H.C. Floresca, A. Covacevich, C.

Pope, R. Piner, M.J. Kim, R.M. Wallace, L. Colombo, R.S. Ruoff, Toward the controlled synthesis of hexagonal boron nitride films, ACS Nano, 6 (2012) 6378–6385.

[22] S.K. Jang, J. Youn, Y.J. Song, S. Lee, Synthesis and Characterization of Hexagonal Boron Nitride as a Gate Dielectric, Sci. Rep., 6 (2016) 30449.

[23] A. Gibb, N. Alem, A. Zettl, Low pressure chemical vapor deposition synthesis of hexagonal boron nitride on polycrystalline metal foils, Phys. Status Solidi, 250 (2013) 2727–2731.

[24] A. Dankert, B. Karpiak, S.P. Dash, Hall sensors batch-fabricated on all-CVD h-BN/graphene/h-BN heterostructures, Sci. Rep., (2017).

[25] M.V. Kamalakar, A. Dankert, J. Bergsten, T. Ive, S.P. Dash, Enhanced tunnel spin injection into graphene using chemical vapor deposited hexagonal boron nitride, Sci. Rep., 4 (2014).

[26] H. Pandey, M. Shaygan, S. Sawallich, S. Kataria, Z. Wang, A. Noculak, M. Otto, M. Nagel, R. Negra, D. Neumaier, M.C. Lemme, All CVD Boron Nitride Encapsulated Graphene FETs with CMOS Compatible Metal Edge Contacts, IEEE Trans. Electron Devices, 65 (2018).

[27] S.M. Kim, A. Hsu, M.H. Park, S.H. Chae, S.J. Yun, J.S. Lee, D.-H. Cho, W. Fang, C. Lee, T. Palacios, M. Dresselhaus, K.K. Kim, Y.H. Lee, J. Kong, Synthesis of large-area multilayer hexagonal boron nitride for high material performance, Nat. Commun., 6 (2015) 8662.

[28] S. Caneva, R.S. Weatherup, B.C. Bayer, R. Blume, A. Cabrero-Vilatela, P. Braeuninger-Weimer, M.B. Martin, R. Wang, C. Baehtz, R. Schloegl, J.C. Meyer, S. Hofmann, Controlling Catalyst Bulk Reservoir Effects for Monolayer Hexagonal Boron Nitride CVD, Nano Lett., 16 (2016) 1250–1261.

[29] Suzuki S, Hibino H, Chemical vapor deposition of hexagonal boron nitride, E-J. Surf. Sci. Nanotech, 10 (2012) 133–138.

[30] S. Sonde, A. Dolocan, N. Lu, C. Corbet, M.J. Kim, E. Tutuc, S.K. Banerjee, L. Colombo, Ultrathin, wafer-scale hexagonal boron nitride on dielectric surfaces by diffusion and segregation mechanism, 2D Mater., 4 (2017) 025052.

[31] A. Ismach, H. Chou, P. Mende, A. Dolocan, R. Addou, S. Aloni, R. Wallace, R. Feenstra, R.S. Ruoff, L. Colombo, Carbon-assisted chemical vapor deposition of hexagonal boron nitride, 2D Mater., 4 (2017).

[32] L.L.J. Lee Y.H., Liu K.K., Lu A.Y., Wu C.Y., Lin C.T., Zhang W., Su C.Y., Hsu C.L., Lin T.W., Wei K.H., Shid Y., Growth selectivity of hexagonal-boron nitride layers on Ni with various crystal orientations, RSC Adv., 2 (2012) 111–115.

[33] H. Cho, S. Park, D.-I. Won, S.O. Kang, S.-S. Pyo, D.-I. Kim, S.M. Kim, H.C. Kim, M.J. Kim, Growth kinetics of white graphene (h-BN) on a planarised Ni foil surface, Sci. Rep., 5 (2015) 11985.

[34] H. Chou, S. Majumder, A. Roy, M. Catalano, P. Zhuang, M. Quevedo-Lopez, L. Colombo, S.K. Banerjee, Dependence of h-BN Film Thickness as Grown on Nickel Single-Crystal Substrates of Different Orientations, ACS Appl. Mater. Interfaces, 10 (2018) 44862–44870.

[35] W.H. Lin, T.H. Chen, J.K. Chang, J.I. Taur, Y.Y. Lo, W.L. Lee, C.S. Chang, W. Bin Su, C.I. Wu, A direct and polymer-free method for transferring graphene grown by chemical vapor deposition to any substrate, ACS Nano, 8 (2014) 1784–1791.

[36] W.Y. Kwong, W.Y. Zhang, Electron-beam assisted platinum deposition as a protective layer for FIB and TEM applications, in: IEEE Int. Symp. Semicond. Manuf. Conf. Proc., 2005.

[37] L. Schué, B. Berini, A.C. Betz, B. Plaçais, F. Ducastelle, J. Barjon, A. Loiseau, Dimensionality effects on the luminescence properties of hBN, Nanoscale, 8 (2016) 6986–6993.

[38] S. Mróz, C. Kozioł, J. Kołaczkiewicz, Carbon and sulphur on the [111] and [001] faces of nickel during thermal treatment in ultra-high vacuum and in an oxygen atmosphere, Vacuum, 26 (1976) 61–65.

[39] P.C. Mende, Q. Gao, A. Ismach, H. Chou, M. Widom, R. Ruoff, L. Colombo, R.M. Feenstra, Characterization of hexagonal boron nitride layers on nickel surfaces by low-energy electron microscopy, Surf. Sci., 659 (2017) 31–42.

[40] B. Dlubak, M.-B. Martin, R.S. Weatherup, H. Yang, C. Deranlot, R. Blume, R. Schloegl, A. Fert, A. Anane, S. Hofmann, P. Seneor, J. Robertson, Graphene-passivated nickel as an oxidation-resistant electrode for spintronics, ACS Nano, 6 (2012) 10930–10934.

[41] K.K. Kim, A. Hsu, X. Jia, S.M. Kim, Y. Shi, M. Hofmann, D. Nezich, J.F. Rodriguez-Nieva, M. Dresselhaus, T. Palacios, J. Kong, Synthesis of monolayer hexagonal boron nitride on Cu foil using chemical vapor deposition, Nano Lett., 12 (2012) 161–166.

[42] Y.-H. Lee, K.-K. Liu, A.-Y. Lu, C.-Y. Wu, C.-T. Lin, W. Zhang, C.-Y. Su, C.-L. Hsu, T.-W. Lin, K.-H. Wei, Y. Shi, L.-J. Li, Growth selectivity of hexagonal-boron nitride layers on Ni with various crystal orientations, RSC Adv., 2 (2012) 111.

[43] V.L.Y. Solozhenko, I.A. Petrusha, A.A. Svirid, V.L. Solozhenko, High Pressure Research: An International Journal Thermal phase stability of rhombohedral boron nitride, An Int. J., 15 (1996) 95–103.

[44] A. Henry, M. Chubarov, Z. Czigány, M. Garbrecht, H. Högberg, Early stages of growth and crystal structure evolution of boron nitride thin films, in: Jpn. J. Appl. Phys., 2016.

[45] P. Sutter, J. Lahiri, P. Zahl, B. Wang, E. Sutter, Scalable synthesis of uniform few-layer hexagonal boron nitride dielectric films, Nano Lett., (2013).

[46] T. Sato, Influence of Monovalent Anions on the Formation of Rhombohedrat Boron Nitride, rBN, Proc.Japan.Acad. Ser.B, 61 (1985) 459–463.

[47] H. Pedersen, B. Alling, H. Högberg, A. Ektarawong, Thermodynamic stability of hexagonal and rhombohedral boron nitride under chemical vapor deposition conditions from van der Waals corrected first principles calculations, J. Vac. Sci. Technol. A, 37 (2019) 040603.

[48] W. Auwärter, H.U. Suter, H. Sachdev, T. Greber, Synthesis of One Monolayer of Hexagonal Boron Nitride on Ni(111) from B-Trichloroborazine (ClBNH)3, Chem. Mater., 16 (2004) 343–345.

[49] R. Geick, C. Perry, G. Rupprecht, Normal Modes in Hexagonal Boron Nitride, Phys. Rev., 146 (1966) 543–547.

[50] J. Liu, Y.K. Vohra, J.T. Tarvin, S.S. Vagarali, Cubic-to-rhombohedral transformation in boron nitride induced by laser heating: In situ Raman-spectroscopy studies, Phys. Rev. B, 51 (1995) 8591.

[51] W.J. Yu, W.M. Lau, S.P. Chan, Z.F. Liu, Q.Q. Zheng, Ab initio study of phase transformations in boron nitride, 20 (n.d.).

[52] M. Chubarov, H. Pedersen, H. Högberg, V. Darakchieva, J. Jensen, P.O.. Persson, A. Henry, Epitaxial CVD growth of sp2-hybridized boron nitride using aluminum nitride as buffer layer, Phys. Status Solidi - Rapid Res. Lett., 5 (2011) 397–399.

[53] M. Chubarov, H. Pedersen, H. Högberg, S. Filippov, J.A.A. Engelbrecht, J. O'Connel, A. Henry, Boron nitride: A new photonic material, Phys. B Condens. Matter, (2014).

[54] R.J. Nemanich, S.A. Solin, R.M. Martin, Light scattering study of boron nitride microcrystals, Phys. Rev. B, 23 (1981) 6348.

[55] R. V. Gorbachev, I. Riaz, R.R. Nair, R. Jalil, L. Britnell, B.D. Belle, E.W. Hill, K.S. Novoselov, K. Watanabe, T. Taniguchi, A.K. Geim, P. Blake, Hunting for monolayer boron nitride: Optical and raman signatures, Small, 7 (2011) 465–468.

[56] K.H. Michel, B. Verberck, Phonon dispersions and piezoelectricity in bulk and multilayers of hexagonal boron nitride, Phys. Rev. B, 83 (2011) 115328.

[57] H.-Z. Zhuang, X.-W. Zou, Z.-Z. Jin, D.-C. Tian, Temperature dependence of Raman spectra of vitreous and molten B2O3, Phys. Rev. B, 55 (1997) R6105.

[58] C.A. Taylor, S.W. Brown, V. Subramaniam, S. Kidner, S.C. Rand, R. Clarke, Observation of near-band-gap luminescence from boron nitride films, Appl. Phys. Lett., 65 (1994) 1251–1253.

[59] P. Jaffrennou, J. Barjon, T. Schmid, L. Museur, A. Kanaev, J.S. Lauret, C.Y. Zhi, C. Tang, Y. Bando, D. Golberg, B. Attal-Tretout, F. Ducastelle, A. Loiseau, Near-band-edge recombinations in multiwalled boron nitride nanotubes: Cathodoluminescence and photoluminescence spectroscopy measurements, Phys. Rev. B, 77 (2008) 235422.

[60] L. Museur, E. Feldbach, A. Kanaev, Defect-related photoluminescence of hexagonal boron nitride, Phys. Rev. B , 78 (2008) 155204.

[61] L. Xu, J. Zhan, J. Hu, Y. Bando, X. Yuan, T. Sekiguchi, M. Mitome, D. Golberg, High-yield synthesis of rhombohedral boron nitride triangular nanoplates, Adv. Mater., 19 (2007) 2141–2144.

Supporting information

Heteroepitaxial growth of sp^2-hybridized boron nitride multilayers on nickel substrates by CVD: the key role of the substrate orientation

H. Prevost[1], A.Andrieux-Ledier[2], N.Dorval[2], F.Fossard[1], J.S.Mérot[1], L. Schué[1,3], A.Plaud[1,3], E. Héripré[4], J.Barjon[3] and A.Loiseau[1]

[1] LEM, UMR 104 CNRS-ONERA, Université Paris Saclay, F-92322 Châtillon - France

[2] DPHY, ONERA, Université Paris Saclay, F-92322 Châtillon - France

[3] GEMaC, CNRS, UVSQ, Université Paris-Saclay, Versailles - France

[4] MSSMat, CNRS - CentraleSupélec, Université Paris-Saclay, 91190 Gif-sur-Yvette - France

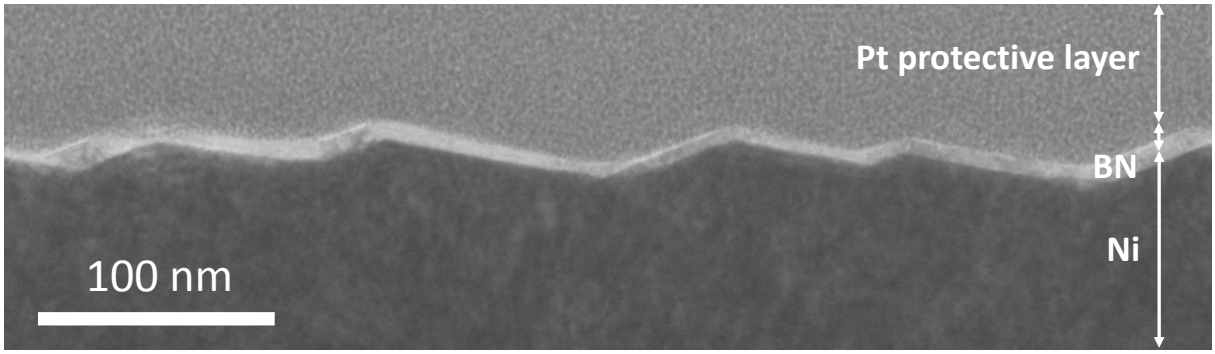

Figure SI1: HRTEM image in edge view configuration of the BN film on Ni(111) surfaces illustrating the presence of step bunches on the nickel . The BN film is conform to its underneath substrate.

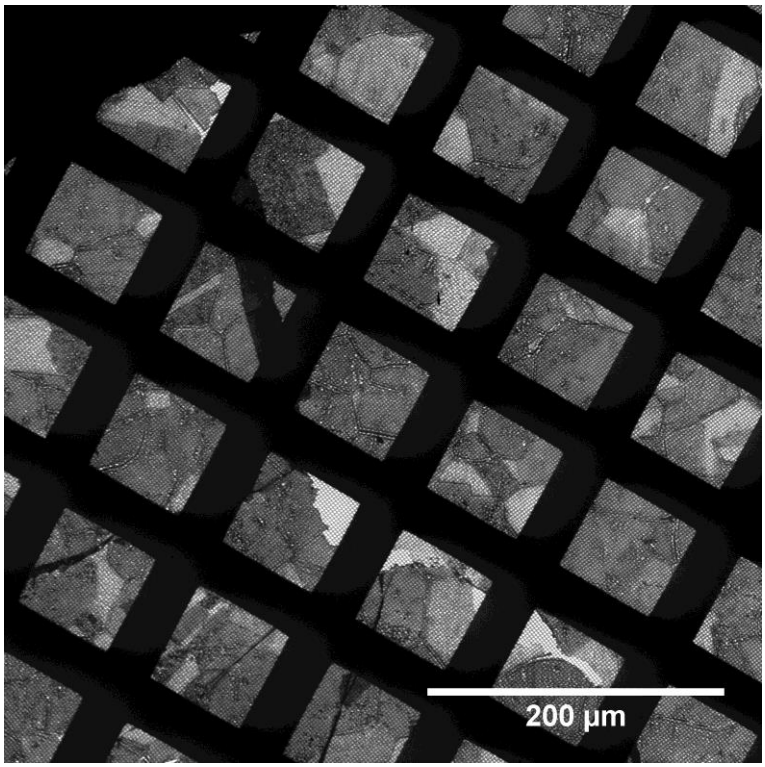

Figure SI2: Low magnification TEM image illustrating the large transfer of the BN film over the whole TEM grid

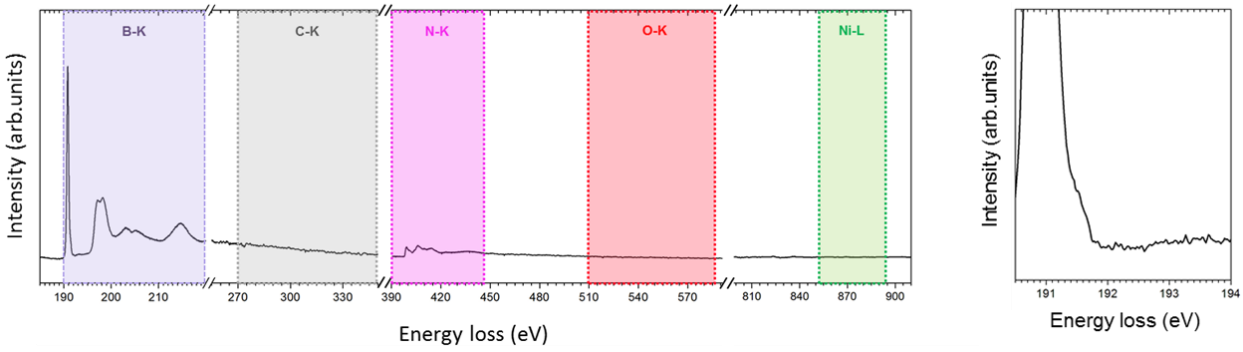

Figure SI3: (a) Typical EELS spectra recording on the boron nitride film showing the B, C, N, O-K edge and Ni-L edge (e) EELS spectra at the B-K edge π^* region

Electron Energy Loss Spectroscopy (EELS) was used to control the chemical composition of the BN film. The spectra were recorded at 40 kV to avoid the formation of defects in BN under electron-beam irradiation [1]. Figure SI3 shows a typical EELS spectrum in the range of 185 to 910 eV. No carbon (280 eV), oxygen (532 eV) K-edges or nickel L-edges (855 eV) appear, indicating the absence of important contamination. The positions of the main feature at boron and nitrogen K-edges (starting at 190.8 and 399.2 eV, respectively) are coherent with the theoretical and experimental values described in the literature for sp^2-hybridized BN [2,3]. At the B K-edge, the presence of the sharp first peak, corresponding to the transition of 1s electron to the empty π^* antibonding orbitals, confirms the sp^2 hybridization [2,4] and the planar bonding. Furthermore, in the π^* region (Figure 2e), we do not observe the presence of additional features relative to the presence of oxygen impurities in substitution of nitrogen atoms in defective BN film [5,6]. As a conclusion, the sp^2 hybridization in layered boron nitride films has been established. The purity of the films is better than the chemical sensitivity of EELS (1 %).

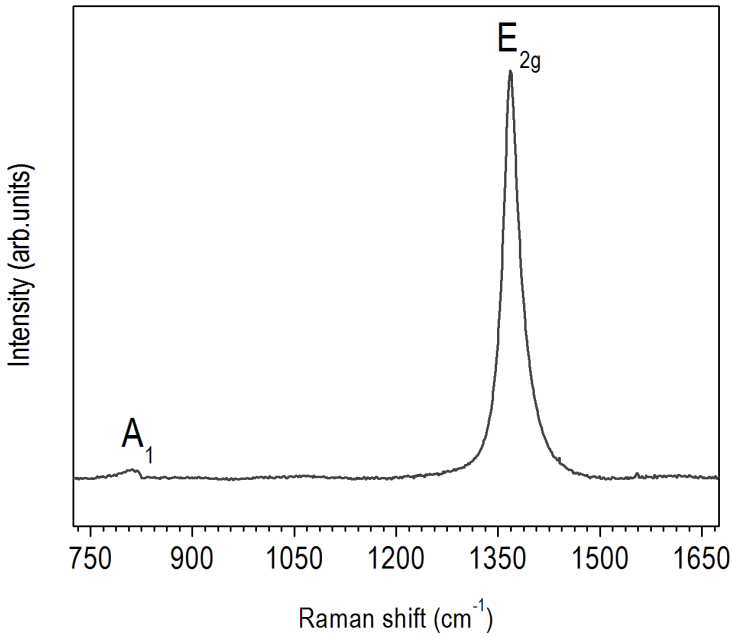

Figure SI4: (a) Typical Raman spectrum recorded on BN film grown on Ni (001) showing both the in–plane vibration mode (E_{2g}) at 1370 cm^{-1} and the layer breathing mode (A_1) at 808 cm^{-1}.

References Supporting Information

[1] J.C. Meyer, A. Chuvilin, G. Algara-Siller, J. Biskupek, U. Kaiser, Selective sputtering and atomic resolution imaging of atomically thin boron nitride membranes, Nano Lett., 9 (2009) 2683–2689.

[2] R. Franke, S. Bender, J. Hormes, A.. Pavlychev, N.. Fominych, A quasi-atomic treatment of chemical and structural effects on K-shell excitations in hexagonal and cubic BN crystals, Chem. Phys., 216 (1997) 243–257.

[3] R. Arenal, M. Kociak, N.J. Zaluzec, High-angular-resolution electron energy loss spectroscopy of hexagonal boron nitride, Appl. Phys. Lett., 90 (2007) 204105.

[4] D.G. McCulloch, D.W.M. Lau, R.J. Nicholls, J.M. Perkins, The near edge structure of cubic boron nitride, Micron, 43 (2012) 43–48.

[5] I. Caretti, I. Jiménez, Point defects in hexagonal BN, BC3 and BCxN compounds studied by x-ray absorption near-edge structure, J. Appl. Phys., 110 (2011) 023511.

[6] S.P. Huber, E. Gullikson, R.W.E. van de Kruijs, F. Bijkerk, D. Prendergast, Oxygen-stabilized triangular defects in hexagonal boron nitride, Phys. Rev. B, 92 (2015) 245310.